

Published in final edited form as:

Structure. 2009 January 14; 17(1): 96–104. doi:10.1016/j.str.2008.11.007.

The Structure of the MAP2K MEK6 Reveals an Autoinhibitory Dimer

Xiaoshan Min^{1, #}, Radha Akella¹, Haixia He¹, John M. Humphreys¹, Susan E. Tsutakawa², Seung-Jae Lee¹, John A. Tainer², Melanie H. Cobb³, and Elizabeth J. Goldsmith^{1, *}

¹Department of Biochemistry, The University of Texas Southwestern Medical Center at Dallas, 5323 Harry Hines Blvd., Dallas, TX 75390-8816, USA

²Lawrence Berkeley National Lab, 1 Cyclotron Road, Berkeley, CA 94720, USA

³Department of Pharmacology, The University of Texas Southwestern Medical Center at Dallas, 5323 Harry Hines Blvd., Dallas, TX 75390-8816, USA

Summary

MAP2Ks are dual-specificity protein kinases functioning at the center of three-tiered MAP kinase modules. The structure of kinase domain of the MAP2K MEK6 with phosphorylation site mimetic aspartic acid mutations (MEK6/ Δ N/DD) has been solved at 2.3 Å resolution. The structure reveals an autoinhibited elongated ellipsoidal dimer. The enzyme adopts an inactive conformation, based upon structural queues, despite the phosphate-mimetic mutations. Gel filtration and small angle X-ray scattering (SAXS) analysis confirm that the crystallographically observed ellipsoidal dimer is a feature of MEK6/ Δ N/DD and full length unphosphorylated wild-type MEK6 in solution. The interface includes the phosphate binding ribbon of each subunit, part of the activation loop, and a rare “Arginine Stack” between symmetry related arginine residues in the N-terminal lobe. The autoinhibited structure likely confers specificity on active MAP2Ks. The dimer may also serve the function in unphosphorylated MEK6 of preventing activation loop phosphorylation by inappropriate kinases.

Introduction

MAP kinase modules are three-tiered kinase cascades that confer switch-like responses to extracellular and stress stimuli in eukaryotes. The modules induce changes in cell program and cell fate in processes such as differentiation, transformation, apoptosis and senescence (Chen et al., 2001; Deng et al., 2004; Johnson and Lapadat, 2002; Pearson et al., 2001). MAP kinase modules are chemically interesting because the central MAP kinase kinases (MEKs) are dual specificity, phosphorylating a Tyr and then a Ser/Thr residue to activate the MAP kinase (Haystead et al., 1992). They are physically interesting because there are numerous distinct MAP kinase modules, which must maintain pathway specificity. Of over a dozen MAP kinases in the human genome, two of the best studied are the extracellular-signal regulated kinase 1/2 (ERK1/2) and its activators MAP/ERK kinases 1

© 2009 Elsevier Inc. All rights reserved.

*Corresponding Author Elizabeth.Goldsmith@UTSouthwestern.edu Phone (214) 645-6376 FAX (214) 645-6387.

#Present address: Amgen Inc., One Amgen Center Drive, Thousand Oaks, CA 91320-1799, USA

Publisher's Disclaimer: This is a PDF file of an unedited manuscript that has been accepted for publication. As a service to our customers we are providing this early version of the manuscript. The manuscript will undergo copyediting, typesetting, and review of the resulting proof before it is published in its final citable form. Please note that during the production process errors may be discovered which could affect the content, and all legal disclaimers that apply to the journal pertain.

Accession Number The coordinates of MEK6/ Δ N/DD have been deposited into the protein data bank with accession number 3ENM.

and 2 (MEK1/2), and p38 MAP kinase isoforms and their activators MEK6 and MEK3 (Raman et al., 2007). Other well-studied pathways include the c-Jun N-terminal kinases (JNKs) activated by MEK4 and MEK7, and ERK5 (Chen et al., 2001) which is activated by MEK5. ERK1/2 are activated by mitogens and growth factors (Raman et al., 2007; Yoon and Seger, 2006). In contrast, p38 isoforms and MEK6 are activated by bacterial liposaccharides, interleukins, tumor necrosis factor, and cellular stresses such as osmotic shock and UV radiation (Zarubin and Han, 2005). ERK5 and MEK5 appear to be activated by a mixture of these signals (Wang and Tournier, 2006). Not surprisingly, MAP kinase module components are drug targets for several classes of diseases, including cancer, inflammation, and degenerative diseases (Sebolt-Leopold and English, 2006).

How pathway fidelity is maintained in MAP kinase modules is being intensively studied, and is now known to involve a variety of docking and scaffolding interactions (Raman et al., 2007; Tanoue and Nishida, 2003). Especially relevant to the present study, it has been shown that docking motifs (D-motifs) in the N-termini of MAP2Ks bind to MAPKs (Bardwell et al., 2003; Bardwell, 2006). Further, a docking sequence in the C-terminus of MAP2Ks, has been shown to mediate interactions with MAP3Ks (Takekawa et al., 2005). This motif has been termed the “DVD” motif, and in MEK6 encompasses the last 23 residues. Thus mammalian MAP2Ks bind both downstream MAPKs and upstream MAP3Ks through docking interactions.

Structural data on MAP kinases is relatively abundant (Goldsmith et al., 2007); structures of full-length inactive and active forms of ERK2, p38 isoforms, and JNK isoforms reveal how MAP kinases are activated by activation loop phosphorylation (Bellon et al., 1999; Canagarajah et al., 1997; Wang et al., 1997; Xie et al., 1998; Zhang et al., 1994). How docking interactions are mediated in MAP kinases has also been studied (Chang et al., 2002; Heo et al., 2004; Liu et al., 2006; Remenyi et al., 2005; Zhou et al., 2006). Docking interactions both engage partners and induce conformational changes that increase activation loop accessibility. These conformational changes are likely to contribute to pathway fidelity, because only kinases and phosphatases that have the right docking motif can unlock the activation loop for chemistry. Structures are also available for MAP3Ks, that reveal some aspects of their regulation by autoinhibition and activation loop phosphorylation. These include the kinase domain structures of B-Raf and TAO2 (Wan et al., 2004; Zhou et al., 2004), and the RAS binding domain of B-Raf (Nassar et al., 1995).

Despite the intrinsic interest of MAP2Ks, as dual specificity kinases assuming a central role in MAP kinase modules, only one structural study has been reported, on the ERK2 activators MEK1/2 (Ohren et al., 2004). To find a fragment that would crystallize, Ohren *et al.* made an N-terminal truncation eliminating the MAPK-binding D-motif. The structures observed were unphosphorylated and inhibitor bound and clearly inactive (discussed below). The MEK1/2 structures also revealed an unexpected dimer. To learn more about the anatomy and regulation of MAP2Ks, in this study, we have determined the structure of the MAP2K MEK6, one of the major activators of the p38 α MAP kinase (Han et al., 1996). Following the protocol of Ohren *et al.*, we made an N-terminal truncation mutant deleting the D-motif. Further, we mutated the two phosphorylation sites of MEK6, Ser207 and Thr211, to aspartic acid to mimic phosphorylation (MEK6/ Δ N/DD), in hopes of seeing the active form of a MAP2K. However, the structure of this mutant reveals a novel autoinhibitory dimer, despite the activating point mutations. The active site is completely blocked in the dimer, and the activation loop is also sequestered in the interface. SAXS analysis and gel filtration reveals that dimers are formed by MEK6/ Δ N/DD and wild-type MEK6. We propose that the dimer interaction presents a mechanism for regulation of both the activity and activation of MEK6.

Results

The construct used for crystallography in this study, MEK6/ Δ N/DD (residues 45-334 of MEK6), contains two phosphorylation mimetic mutations in the activation loop (Ser207Asp and Thr211Asp), and lacks the docking motif for substrate p38 α (Enslin et al., 2000). In the context of full length MEK6, the aspartic acid mutants confer activity toward its substrate p38 α as is the case for MEK1/2 (Huang et al., 1995). The turn over numbers for full-length MEK6/DD and wild type doubly phosphorylated full length MEK6 are 12.8 ± 0.6 and 8.0 ± 0.1 , respectively (Humphreys and Goldsmith, unpublished data).

The structure was solved by single-wavelength anomalous dispersion (SAD) from a complete data set collected on a single selenomethionine incorporated protein crystal and refined against 2.35 Å resolution x-ray data. The final structure was refined in REFMAC5 (Murshudov et al., 1997) to an R-factor of 19.6% (R_{free} 24.7%) with reasonable stereochemistry (Table 1). The protein crystallized in space group P3₂21, with four subunits in the asymmetric unit. The four subunits form two tight dimers shown in Figure 1A (left panel). One of the two dimers is shown in the right panel of Figure 1A. The individual chains are very similar. In all the four chains, part of the activation loop (Val208-Cys216) is disordered. A TLS refinement was performed with four TLS parameters per chain (Painter and Merritt, 2006). The B-factors were uniformly elevated, indicative of motion of the individual chains. Nevertheless, the pairwise root-mean-square deviation (r.m.s.d.) ranged between 0.6 and 0.8 Å among the four subunits. The model contains 1111 residues, 4 sulfate ions and 331 water molecules.

The MEK6 monomer structure

MEK6 belongs to the STE group of protein kinases (Manning and Davis, 2003), and the MEK6/ Δ N/DD construct used is similar in length to another STE group kinase TAO2 (TAO2 (1-320)), the structure of which was solved in an active conformation (Zhou et al., 2004). As with TAO2, the MEK6/ Δ N/DD subunit adopts a bi-lobal fold, similar to other protein kinases (Jones et al., 1997; Knighton et al., 1991) (Figure 1B), with two additional helices, (J and K) at the C-terminus. The N-terminal lobe of MEK6/ Δ N/DD is comprised of a β -sheet and one long helix (helix C); the C-terminal lobe is helical. Comparison of MEK6 to active TAO2 reveals dramatic differences; suggestive that MEK6 adopts an inactive structure despite the phosphomimetic mutations. As in protein kinases generally, the N-terminal lobe β -sheet of TAO2 consists of 5 strands (Figure 1B). (The first two strands of the β -sheet are also referred to as the ATP phosphate binding ribbon or P-loop (Jones et al., 1997)). In contrast to TAO2, the phosphate binding ribbon in MEK6 is formed into a large loop between Ile56 and Glu68, reminiscent of an Ω -loop (Leszczynski and Rose, 1986). At the C-terminus of this Ω -loop, Glu68 makes an ion-pair with the catalytic lysine (Lys82) in β -strand 3.

The activation loop of MEK6/ Δ N/DD exhibits hallmarks of a kinase-inactive conformation. The DFG motif (subdomain VII) at the beginning of the activation loop adopts a modified “DFG-out” configuration, which is present in some inactive kinases and inhibitor complexes (Wroblewski and Doweyko, 2005) (Figure 1B). Asp197 of the DFG occupies the pocket normally held by the Phe198, and accepts a hydrogen bond from a serine in helix C, Ser103 (not shown). Residues Ile200 to Tyr203 of the activation loop make one turn of helix (Figures 1B). This helix, together with Phe198 of the DFG is wedged between the N-terminal lobe β -sheet and helix C. The location of this helix prevents the formation of an ion pair between the catalytic Lys82 in β -strand 3 and Asp99 from helix-C, expected for an active kinase (Huse and Kuriyan, 2002). Similarly in MEK1/2, the small helix at the N-terminus of the activation loop also disrupts the Lys-Asp ion-pair (Ohren et al., 2004). The last residue of the activation loop that is fully visible is Ser207Asp (phosphomimetic

mutation to aspartic acid). The activation loop is disordered from Val208 through Cys216, including the phosphorylation site Thr211Asp (mutated to aspartic acid). In active kinases, Cys216 would be expected to contact the catalytic loop residues Asp171 and Lys181 (Goldsmith et al., 2007), but is instead disordered. The other residues in the activation loop, Lys217, Pro218, and Tyr219, are visible, but deviate from expected positions (see Figure 1B). The degree of remodeling of the C-terminus of the activation loop is similar to that of inactive PAK1, another STE group kinase (Lei et al., 2000; Zhou et al., 2004).

In the C-terminal lobe, following the kinase-conserved helix I, MEK6 has two further helices, J and K, that extend nearly to the C-terminus of the chain, and pack against the kinase core. The first helix (J), residues Pro312-Lys320, packs across helix E and the second helix (K), residues Val324-Leu332, binds in the groove between helices D and E the β 7- β 8 hairpin turn (Figure 1B). (In MAPKs, the homologous groove binds D-motifs). The last two residues (Gly334 and Asp335), which are conserved in MEK3/6 subgroup, are not visible in the electron density. Helices J and K adopt nearly identical positions to the same helices in MEK1/2 (Ohren et al., 2004). The “DVD docking site” in MAP2Ks that mediates interactions with MAP3Ks (Takekawa et al., 2005) encompasses part of helix J and all of helix K. Takekawa *et al.* showed that His317, Thr322, Val324, Phe327, Val328, and Ile331 of MEK6 (shown as blue balls in Figure 1C) affect interactions with MAP3Ks, including TAO2, when mutated. Leu332 (green ball), which follows these DVD residues, also forms contacts in the subunit interface (discussed below).

The structure offers clues concerning the residues likely to be involved in recognition of the activation loop Ser/Thr phosphorylation sites of MAP2Ks in their phosphorylated active configuration. Following the activation loop (and P+1 site), subdomain VIII of MAP2Ks has a conserved motif PYMAPER. The arginine at terminus of this sequence, Arg224, is unique to MAP2Ks. Here we observe that it is nearby Arg178 in subdomain IV (Figure 1D), the conserved arginine involved in phosphothreonine or phosphotyrosine binding in active kinases (Hubbard, 1997). Thus, this arginine may be involved in S*/T* recognition in MEK6/S*T*. Another feature is that the residues forming the loop between ²¹⁸PYMAPER²²⁴ and helix F (Asn226 to Ser235) are not tightly packed on the kinase core, and Leu229 faces solvent, creating an open conformation of the loop between the PYMAPER motif and helix F. This extended structure arises from an insert of three residues in the MEK6/MEK3 subgroup, as discussed below.

The MEK6 dimer interface

The four subunits of the crystallographic asymmetric unit form two very similar two-fold symmetric tight dimers (left panel of Figure 1A). The dimer brings the N-termini of the two subunits together creating an elongated ellipsoid (right panel of Figure 1A) that buries 1500 Å² of surface. In the interface, the distorted Ω -loop-shaped phosphate binding ribbon of one subunit binds in the ATP binding site of the opposite subunit (Figure 2A). Tyr64, which in active kinases is at the apex of the phosphate binding ribbon, occupies the nucleotide binding site of the opposite subunit. The backbone carbonyl groups of Tyr64 and Ala63 accept hydrogen bonds from the catalytic Lys82'N ζ . (ζ denotes second subunit) and the nitrogen atom in Val67 makes a hydrogen bond to the side chain oxygen atom (O δ 1) in Asp206' in the activation loop. The Ω -loop also make contacts with the opposite C-terminus where Leu59' contacts Leu332 (Figure 2A). Weak hydrogen bonds also link the Ω -loop and the crossover connection at the back of the active site (not shown). Overall, the interactions between the two subunits appear to both render the protein inactive and limit the accessibility of the activation loop phosphorylation sites (blue spheres in Figure 1A) toward other kinases or phosphatases.

The dimer interface also involves the linker between β -strand 3 and helix C and the loop between β -strand 4 and β -strand 5 (Figure 2A). An unusual “Arginine Stack” is found in the center of this interaction (Figure 2B). Arg83, that is located at the end of the β -strand 3 stacks with its symmetry mate. This Arginine Stack is stabilized by ion pair interactions with Asp124' from the loop between β -strand 4 and β -strand 5 of the opposite subunit (and the symmetry related interaction between Arg83' and Asp124). Arginine stacks are rare in protein structures but are thought to be stabilizing the interactions (Magalhaes et al., 1994). An Arginine Stack very similar to this one was recently found to be involved in the synaptotagmin switch mechanism (Fuson et al., 2007).

MEK6 oligomerization in solution

To obtain information on the molecular envelope and state of oligomerization in solution, small-angle x-ray scattering (SAXS) was performed on MEK6/ Δ N/DD at the SIBYLS beamline in the Advanced Light Source (Putnam et al., 2007; Tsutakawa et al., 2007). The shape of the scattering curve and electron pair distribution (Figure 3A and B) are consistent with an elongated ellipsoid (Koch et al., 2003). The Guinier plots were linear, an indication of monodispersity of the sample (Figure 3C). The radius of gyration from the GNOM analysis was 38 Å. Based on data below, the scattering vector $q = 0.2 \text{ \AA}^{-1}$, the Porod volume (hydrated volume) for MEK6/ Δ N/DD is $132,000 \text{ \AA}^3$, providing an approximate molecular mass of 79,000 Daltons. The calculated MW of each MEK6/ Δ N/DD including the N-terminal hexa-His tag is approximately 36 kD. Thus, the Porod volume is consistent with a dimer. Further, *ab initio* analysis in P1 symmetry by the program DAMMIN revealed an elongated structure (Figure 3D) of the same volume. The apparent P2 symmetry, when no symmetry was enforced, is again consistent with a dimer.

Both MEK6/ Δ N/DD and full-length MEK6 also elute as dimers on Superdex75 16/60 gel filtration column (elution volume ~58 ml). ATP (1mM) in the column buffer causes the elution volume to increase (Figure 4) as observed by analytical gel filtration Superdex-200 10/300, suggestive of a change in the dimer-monomer equilibrium within a physiologically relevant concentration range (Gribble et al., 2000; Marjanovic et al., 1993).

The sequence conservation of the subunit interface

A multiple sequence alignment of MAP2Ks given in Figure 5A revealed that many residues in the observed MEK6 dimer are conserved in the MEK6/MEK3 subgroup, but are not conserved in MEK1/2. Tyr64, Arg83, Asp124 and Leu332 are conserved residues in the interface. Further, Tyr203, in the activation loop and interface is conserved in MEK3/6 subgroup. Single point mutations of the conserved residues (orange balls in Figure 1C) in the interface including Arg83 involved in the arginine stack (discussed above) did not show any strong effect on the dimer. A double mutant, D124A/W126S was synthesized, which showed a slight change in the elution volume on a Superdex-200 10/300 gel-filtration, indicative of a shift towards a monomer (Figure 4). We also tested the activity of these MEK6/ Δ N/DD mutants toward p38 α and found that none of them rescued the low activity of MEK6/ Δ N/DD (data not shown). These data further support the idea that the docking motif of MEK6 is required for activity towards its substrate MAPK (Bardwell, 2006).

Comparison of MEK6 with MEK1/2

Crystallographic studies of MEK1/2 were on inactive, unphosphorylated MEK1/2 (Ohren et al., 2004). There are several interesting parallels between inactive MEK1/2 (N-terminal truncation mutant) and MEK6/ Δ N/DD, however. First, there are similarities in secondary structure arrangements. The activation loops of both are formed into a small helix that makes most of its contacts with the N-terminal lobe, between the β -sheet and helix C. The

placement of Arg224 in the PYMAPER sequence is similar in both structures, in close proximity to the phosphorylation sites in active kinases (Figure 1D). In MEK1/2, the loop following the PYMAPER sequence is shorter by 3 residues and not quite as extended as in MEK6. At the C-terminus, MEK1/2 have very similar C-terminal helices (J and K). On the other hand, MEK1/2 have a normal phosphate binding ribbon, in contrast to the Ω -loop observed in MEK6/ Δ N/DD.

A second similarity is that both MEK6 and MEK1/2 form dimers. However, the dimers are mediated by completely different contacts (Figure 5B). In MEK6, most of the interactions are between the N-terminal domains as discussed above, while in MEK1/2, the interface is near the helix G and the activation loop. Further, the MEK6 dimer adopts an anti-parallel configuration while MEK1/2 form a parallel configuration. Residues that form the interfaces are conserved in each subgroup (Figure 5A) but not between subgroups. In the MEK1/2 dimers, access to the active site is blocked for macromolecules, although not for small molecules. Further access to the activation loop by macromolecules is also partially restricted in MEK1/2. These data suggest similar roles for the MEK1/2 and MEK6 dimers in regulation of their activity and phosphorylation site processing by kinases and phosphatases.

Discussion

Recent structural studies have revealed that many protein kinases forms distinctive higher order assemblies with altered activities. For example, two recent studies, one in EGFR (Zhang et al., 2006) and the another on antiviral protein kinase PKR (Dey et al., 2005) implicate dimerization in the activation mechanism. Our data suggest that MEK6 forms an autoinhibitory dimer in the absence of its own substrates or other interacting partners. The elongated ellipsoidal dimer observed crystallographically for MEK6/ Δ N/DD was also found for full length wild-type MEK6 in SAXS analysis showing that the dimer is a feature of full length MEK6. The primary function of the autoinhibitory dimer may be to maintain MEK6 in an inactive form in the absence of its substrates. So far, it is unclear how the dimer is broken by substrate interactions. The dimer may also have a role in restricting the activation of MEK6. The MEK6 activation loop, although partially disordered, is surrounded by protein and is inaccessible to macromolecules. The docking motif (DVD motif) for MAP3Ks identified by Takekawa et al (Takekawa et al., 2005) is at the C-terminus of MEK6. Since the C-terminal residue Leu332 is in the dimer interface, it is apparent that interactions with a MAP3K should disrupt the MEK6 dimer, thus perhaps making the activation loop of MEK6 more available for processing by the MAP3K. Thus it is possible that this inactive dimer has a role both in the phosphorylated and unphosphorylated forms. In the active phosphorylated form, it restricts access to inappropriate substrates. In the unphosphorylated form, it prevents activation by inappropriate kinases.

It is interesting that MEK1/2/ Δ N, inhibitor bound and unphosphorylated, also form dimers. Although the interface is completely different from MEK6 (Ohren et al., 2004), the MEK1/2 dimers also block access of the substrate binding site and the activation loop from macromolecules, perhaps again having a role in regulating both activity and activation. It is intriguing in this regard that in both MEK1/2 and MEK6, the phosphorylation sites are in the dimer interface but not visible in these inactive dimers. Since the MEK1/2 study was done on unphosphorylated MEK1/2 and our study was done with phosphorylation site mimetics, apparently, the stability of the dimers may not depend on phosphorylation status in either case.

This autoinhibitory dimer of MEK6, and by inference MEK1/2 dimers, add to a growing list of unanticipated allosteric regulatory mechanisms that confer pathway specificity in MAP kinase modules and other protein kinases (Goldsmith et al., 2007), (Biondi and Nebreda,

2003). Crystal structural studies from several laboratories, including ours, previously showed that the docking interaction between MAP2Ks and MAPKs works allosterically to make the activation loop of MAPKs available for processing by kinases and phosphatases (Chang et al., 2002), (Zhou et al., 2006). Here, we see that the MAP2K adopts an inactive configuration in the absence of its substrates, and again the activation loop is sequestered from the action of inappropriate kinases and phosphatases. The autoinhibited dimer observed for MEK6 is also reminiscent of the phenomenon of autoinhibition in MAP3Ks mediated by regulatory domains (Takekawa et al., 2005). We look forward to more data on the significance of dimerization to activity of MAP2Ks in the context of full length wild-type proteins, and to fully explore the role of individual residues in the dimer-monomer equilibrium.

Experimental Procedures

Protein Expression and crystallization

Human MEK6 (residues 41-334) was cloned into a pHisParallel vector using NcoI and SpeI sites (Sheffield, 1999). Point mutations Ser207D and Thr211D and others were introduced using Quikchange kit (Stratagene). The MEK6/ Δ N/DD protein was expressed in Rosetta 2 cells (Novagen). The cells were induced with 0.5 mM IPTG at OD 0.7 and the protein was expressed for 12 hour at 18°C. Cells were lysed in two passes through an Avestin cell disruptor. The lysate was cleared by centrifugation at 35,000 \times g for 1 hr. The supernatant was applied to a Ni sepharose column (GE life sciences) precharged with 0.1 mM NiSO₄ and protein eluted with 250 mM imidazole. The protein was further purified by anion exchange chromatography on MonoQ HR 5/5 column (GE life sciences) using a linear gradient and size exclusion chromatography on a Superdex 75 16/60 column (GE life sciences). The final buffer was 30 mM Hepes, 100 mM NaCl, 1 mM EDTA, 1 mM DTT, 1mM TCEP (tris(2-carboxyethylphosphene), Sigma). Protein was concentrated to 12 mg/ml using Amicon concentrator. Prior to crystallization trials, 0.05% β -octyl glucoside was added. The Seleno-methionine incorporated protein was expressed in *met* auxotrophic strain B834 (Novagen) grown in minimum media supplemented with selenomethionine and other nutrients (Doublie et al., 1994) and purified using the same protocol as the native protein. The crystals of both native protein and seleno-methionine incorporated protein were grown using hanging drop method. The well solution contains 1.6 M Li₂SO₄, and 0.1 M Tris, pH 8.0. The crystals reached 0.2 \times 0.2 \times 0.15 millimeters in one week. The crystallization drop was supplemented with 20% glycerol and the crystals were frozen in liquid propane before data collection.

Data collection and structure solution

A single wavelength anomalous data set for the seleno-methionine incorporated protein crystal was collected at beamline 19-BM at Advanced Photon Source at Argonne National Laboratory. The data were integrated and scaled using the HKL2000 program (Otwinowski, 1997). 39 out of 48 possible selenomethionine sites were located using program SHELXD (Schneider and Sheldrick, 2002). The phases were improved further by solvent flattening using CNS program (Brunger et al., 1998). The initial model was constructed using a combination of manual tracing and Arp/wARP auto tracing (Perrakis et al., 1999). The model was refined using program REFMAC5 (Murshudov et al., 1997) in the CCP4 software suite (Collaborative Computing Project, 1994), followed by iterative rounds of manual building with program O (Jones et al., 1991). Within REFMAC5 rigid body refinement was carried out separating the domains between Glu130 and Leu131 of the four monomers in the asymmetric unit. The final structure was refined to R factor of 19.6% (R free 24.7%).

Small angle X-ray scattering

SAXS data was collected on MEK6/ Δ N/DD, purified by gel filtration, on the SIBYLS beam line at the Advanced Light Source in Lawrence Berkeley National Laboratory with a Mar165 CCD detector. Scattering data was collected with 1.11587 Å wavelength X-ray radiation, and processed by the Svergun software suite (Svergun et al., 2001). Three protein concentrations (10mg/ml, 5mg/ml and 2.5mg/ml) and the equivalent gel filtration buffer were exposed for 7 seconds and 70 seconds at room temperature. The program OGRE was used to subtract protein from buffer frames taken for the same length of exposure and account for the sample-detector distance and wavelength. Guinier analysis detected a small but significant radiation sensitivity that caused eventual sample aggregation, so only the first short exposure was used for analyses. The most concentrated sample, with the best signal to noise ratio, was superimposable on lower concentrations. These data were processed with PRIMUS of the ATSAS 2.1 suite (Svergun et al., 2001) for the Guinier and Porod analyses. This data was further processed using the regularization technique in GNOM in which the pairwise electron distribution function (Patterson function) was obtained from the transform of the scattering function with the D_{max} of 140 Å. Ten *ab-initio* shape determination runs were done using DAMMIN (Svergun et al., 2001), which does not require input of the molecular mass and therefore is independent of user bias. The χ^2 from the DAMMIN log files (1.031 – 1.033) reflect a good match of the individual *ab-initio* shape predictions to the scattering curves. Averaged output of the 10 runs were filtered using DAMAVER (Svergun et al., 2001). Models were superimposable with the observed DAMFILT shape shown in Fig. 3D.

Kinase Assays

The phosphorylation of p38 α and myelin basic protein (MBP) by various MEK6 enzymes was conducted using the standard [γ - 32 P] ATP kinase assay conditions. All kinase assays were carried out under the standard conditions of 20 mM HEPES pH 7.4, 20mM MgCl₂, 2.5 mM ATP and substrate in a final volume of 100 μ L at 30°C. For radiolabeled products, 5-10 μ Ci of [γ - 32 P]ATP per reaction was mixed with the cold ATP. All reactions were initiated by the addition of enzyme after equilibration for 5 min at 30°C. Typical assays used 20 pmoles of MEK6 and 2500pmoles of p38 α or 2000pmoles of MBP. Assay termination and phosphorylation measurement was accomplished using protocols described previously (Braun et al., 1984; Racker, 1991). Reactions were terminated at desired time points by spotting aliquots on 3MM filter paper followed by immediate immersion in termination solution (10% trichloroacetic acid and 10 mM pyrophosphate). Washing with fresh termination solution was followed by autoradiography.

Acknowledgments

We thank Drs. Diana Tomchick and Mischa Machius and the staff at Argonne National Laboratory for help in Synchrotron data collection. We thank Dr. Luke Rice for help in analytical gel filtration. We thank beamline scientist Michal Hammel for aiding expert SAXS analyses. This research was supported by grants from the NIH DK46993 and funding I1128 and I1243 from the Welch Foundation. The U.S. Department of Energy, Office of Biological and Environmental Research, under Contract No.W-31-109-ENG-38, supported use of the Argonne National Laboratory Structural Biology Center beamlines at the Advanced Photon Source. X-ray scattering technologies at the Lawrence Berkeley National Laboratory SIBYLS beamline of the Advanced Light Source (ALS) are supported by the DOE program Integrated Diffraction Analysis Technologies (IDAT) under Contract DE-AC02-05CH11231 with the U.S. Department of Energy. Applications of SAXS and crystallography at the ALS relevant to human cancers are supported in part by National Cancer Institute grant CA92584.

References

- Bardwell AJ, Abdollahi M, Bardwell L. Docking sites on mitogen-activated protein kinase (MAPK) kinases, MAPK phosphatases and the Elk-1 transcription factor compete for MAPK binding and are crucial for enzymic activity. *Biochem J*. 2003; 370:1077–1085. [PubMed: 12529172]
- Bardwell L. Mechanisms of MAPK signalling specificity. *Biochem Soc Trans*. 2006; 34:837–841. [PubMed: 17052210]
- Bellon S, Fitzgibbon MJ, Fox T, Hsiao HM, Wilson KP. The structure of phosphorylated p38gamma is monomeric and reveals a conserved activation-loop conformation. *Structure*. 1999; 7:1057–1065. [PubMed: 10508788]
- Biondi RM, Nebreda AR. Signalling specificity of Ser/Thr protein kinases through docking-site-mediated interactions. *Biochem J*. 2003; 372:1–13. [PubMed: 12600273]
- Braun S, Raymond WE, Racker E. Synthetic tyrosine polymers as substrates and inhibitors of tyrosine-specific protein kinases. *J Biol Chem*. 1984; 259:2051–2054. [PubMed: 6538195]
- Brunger AT, Adams PD, Clore GM, DeLano WL, Gros P, Grosse-Kunstleve RW, Jiang JS, Kuszewski J, Nilges M, Pannu NS, Read RJ, Rice LM, Simonson T, Warren GL. Crystallography & NMR system: A new software suite for macromolecular structure determination. *Acta Crystallogr D Biol Crystallogr*. 1998; 54(Pt 5):905–921. [PubMed: 9757107]
- Canagarajah BJ, Khokhlatchev A, Cobb MH, Goldsmith EJ. Activation mechanism of the MAP kinase ERK2 by dual phosphorylation. *Cell*. 1997; 90:859–869. [PubMed: 9298898]
- Chang CI, Xu BE, Akella R, Cobb MH, Goldsmith EJ. Crystal structures of MAP kinase p38 complexed to the docking sites on its nuclear substrate MEF2A and activator MKK3b. *Mol Cell*. 2002; 9:1241–1249. [PubMed: 12086621]
- Chen Z, Gibson TB, Robinson F, Silvestro L, Pearson G, Xu B, Wright A, Vanderbilt C, Cobb MH. MAP kinases. *Chem Rev*. 2001; 101:2449–2476. [PubMed: 11749383]
- Collaborative Computing Project, N. The CCP4 suite: programs for protein crystallography. *Acta Crystallography*. 1994; D50:760–763.
- DeLano, WL. The PyMOL Molecular Graphics System. Delano Scientific; San Carlos, CA, USA: 2002.
- Deng Q, Liao R, Wu BL, Sun P. High intensity ras signaling induces premature senescence by activating p38 pathway in primary human fibroblasts. *J Biol Chem*. 2004; 279:1050–1059. [PubMed: 14593117]
- Dey M, Cao C, Dar AC, Tamura T, Ozato K, Sicheri F, Dever TE. Mechanistic link between PKR dimerization, autophosphorylation, and eIF2alpha substrate recognition. *Cell*. 2005; 122:901–913. [PubMed: 16179259]
- Doublet S, Xiang S, Gilmore CJ, Carter CW Jr. Overcoming non-isomorphism by phase permutation and likelihood scoring: Solution of the TrpRS crystal structure. *Acta Cryst*. 1994; A50:164–182.
- Enslin H, Branch DM, Davis RJ. Molecular determinants that mediate selective activation of p38 MAP kinase isoforms. *EMBO J*. 2000; 19:1301–1311. [PubMed: 10716930]
- Fuson KL, Montes M, Robert JJ, Sutton RB. Structure of human synaptotagmin 1 C2AB in the absence of Ca²⁺ reveals a novel domain association. *Biochemistry*. 2007; 46:13041–13048. [PubMed: 17956130]
- Goldsmith EJ, Akella R, Min X, Zhou T, Humphreys JM. Substrate and docking interactions in serine/threonine protein kinases. *Chem Rev*. 2007; 107:5065–5081. [PubMed: 17949044]
- Gribble FM, Loussouarn G, Tucker SJ, Zhao C, Nichols CG, Ashcroft FM. A novel method for measurement of submembrane ATP concentration. *J Biol Chem*. 2000; 275:30046–30049. [PubMed: 10866996]
- Han J, Lee JD, Jiang Y, Li Z, Feng L, Ulevitch RJ. Characterization of the structure and function of a novel MAP kinase kinase (MKK6). *J Biol Chem*. 1996; 271:2886–2891. [PubMed: 8621675]
- Haystead TA, Dent P, Wu J, Haystead CM, Sturgill TW. Ordered phosphorylation of p42mapk by MAP kinase kinase. *FEBS Lett*. 1992; 306:17–22. [PubMed: 1628739]
- Heo YS, Kim SK, Seo CI, Kim YK, Sung BJ, Lee HS, Lee JI, Park SY, Kim JH, Hwang KY, Hyun YL, Jeon YH, Ro S, Cho JM, Lee TG, Yang CH. Structural basis for the selective inhibition of

- JNK1 by the scaffolding protein JIP1 and SP600125. *Embo J.* 2004; 23:2185–2195. [PubMed: 15141161]
- Huang W, Kessler DS, Erikson RL. Biochemical and biological analysis of Mek1 phosphorylation site mutants. *Mol Biol Cell.* 1995; 6:237–245. [PubMed: 7612960]
- Hubbard SR. Crystal structure of the activated insulin receptor tyrosine kinase in complex with peptide substrate and ATP analog. *EMBO J.* 1997; 16:5572–5581. [PubMed: 9312016]
- Huse M, Kuriyan J. The conformational plasticity of protein kinases. *Cell.* 2002; 109:275–282. [PubMed: 12015977]
- Johnson GL, Lapadat R. Mitogen-activated protein kinase pathways mediated by ERK, JNK, and p38 protein kinases. *Science.* 2002; 298:1911–1912. [PubMed: 12471242]
- Jones G, Willett P, Glen RC, Leach AR, Taylor R. Development and validation of a genetic algorithm for flexible docking. *J Mol Biol.* 1997; 267:727–748. [PubMed: 9126849]
- Jones TA, Zou JY, Cowan SW, Kjeldgaard. Improved methods for building protein models in electron density maps and the location of errors in these models. *Acta Crystallogr A.* 1991; 47(Pt 2):110–119. [PubMed: 2025413]
- Knighton DR, Zheng J, Ten Eyck LF, Ashford VA, Xuong N-H, Taylor SS, Sowadski JM. Crystal structure of the catalytic subunit of cyclic adenosine monophosphate-dependent protein kinase. *Science.* 1991; 253:407–413. [PubMed: 1862342]
- Koch MH, Vachette P, Svergun DI. Small-angle scattering: a view on the properties, structures and structural changes of biological macromolecules in solution. *Q Rev Biophys.* 2003; 36:147–227. [PubMed: 14686102]
- Lei M, Lu W, Meng W, Parrini MC, Eck MJ, Mayer BJ, Harrison SC. Structure of PAK1 in an autoinhibited conformation reveals a multistage activation switch. *Cell.* 2000; 102:387–397. [PubMed: 10975528]
- Leszczynski JF, Rose GD. Loops in globular proteins: a novel category of secondary structure. *Science.* 1986; 234:849–855. [PubMed: 3775366]
- Liu S, Sun JP, Zhou B, Zhang ZY. Structural basis of docking interactions between ERK2 and MAP kinase phosphatase 3. *Proc Natl Acad Sci U S A.* 2006; 103:5326–5331. [PubMed: 16567630]
- Magalhaes A, Maigret B, Hoflack J, Gomes JN, Scheraga HA. Contribution of unusual arginine-arginine short-range interactions to stabilization and recognition in proteins. *J Protein Chem.* 1994; 13:195–215. [PubMed: 8060493]
- Manning AM, Davis RJ. Targeting JNK for therapeutic benefit: from junk to gold? *Nat Rev Drug Discov.* 2003; 2:554–565. [PubMed: 12815381]
- Marjanovic M, Gregory C, Ghosh P, Willis JS, Dawson MJ. A comparison of effect of temperature on phosphorus metabolites, pH and Mg²⁺ in human and ground squirrel red cells. *J Physiol.* 1993; 470:559–574. [PubMed: 8308744]
- Murshudov GN, Vagin AA, Dodson EJ. Refinement of macromolecular structures by the maximum-likelihood method. *Acta Crystallogr D Biol Crystallogr.* 1997; 53:240–255. [PubMed: 15299926]
- Nassar N, Horn G, Herrmann C, Scherer A, McCormick F, Wittinghofer A. The 2.2 Å crystal structure of the Ras-binding domain of the serine/threonine kinase c-Raf1 in complex with Rap1A and a GTP analogue. *Nature.* 1995; 375:554–560. [PubMed: 7791872]
- Ohren JF, Chen H, Pavlovsky A, Whitehead C, Zhang E, Kuffa P, Yan C, McConnell P, Spessard C, Banotai C, Mueller WT, Delaney A, Omer C, Sebolt-Leopold J, Dudley DT, Leung IK, Flamme C, Warmus J, Kaufman M, Barrett S, Teclé H, Hasemann CA. Structures of human MAP kinase kinase 1 (MEK1) and MEK2 describe novel noncompetitive kinase inhibition. *Nat Struct Mol Biol.* 2004; 11:1192–1197. [PubMed: 15543157]
- Otwinowski Z, Minor W. Processing of X-ray diffraction data collected in oscillation mode. *Methods Enzymol.* 1997; 276:307–326.
- Painter J, Merritt EA. Optimal description of a protein structure in terms of multiple groups undergoing TLS motion. *Acta Crystallogr D Biol Crystallogr.* 2006; 62:439–450. [PubMed: 16552146]
- Pearson G, Robinson F, Beers Gibson T, Xu BE, Karandikar M, Berman K, Cobb MH. Mitogen-activated protein (MAP) kinase pathways: regulation and physiological functions. *Endocr Rev.* 2001; 22:153–183. [PubMed: 11294822]

- Perrakis A, Morris R, Lamzin VS. Automated protein model building combined with iterative structure refinement. *Nat Struct Biol.* 1999; 6:458–463. [PubMed: 10331874]
- Putnam CD, Hammel M, Hura GL, Tainer JA. X-ray solution scattering (SAXS) combined with crystallography and computation: defining accurate macromolecular structures, conformations and assemblies in solution. *Q Rev Biophys.* 2007; 40:191–285. [PubMed: 18078545]
- Racker E. Use of synthetic amino acid polymers for assay of protein-tyrosine and protein-serine kinases. *Methods Enzymol.* 1991; 200:107–111. [PubMed: 1835510]
- Raman M, Chen W, Cobb MH. Differential regulation and properties of MAPKs. *Oncogene.* 2007; 26:3100–3112. [PubMed: 17496909]
- Remenyi A, Good MC, Bhattacharyya RP, Lim WA. The role of docking interactions in mediating signaling input, output, and discrimination in the yeast MAPK network. *Mol Cell.* 2005; 20:951–962. [PubMed: 16364919]
- Schneider TR, Sheldrick GM. Substructure solution with SHELXD. *Acta Crystallographica Section D.* 2002; 58:1772–1779.
- Sebolt-Leopold JS, English JM. Mechanisms of drug inhibition of signalling molecules. *Nature.* 2006; 441:457–462. [PubMed: 16724058]
- Sheffield P, Garrard S, Derewenda Z. Overcoming Expression and Purification Problems of RhoGDI Using a Family of Parallel Expression Vectors. *Protein Expression and Purification.* 1999; 15:34–39. [PubMed: 10024467]
- Svergun DI, Petoukhov MV, Koch MH. Determination of domain structure of proteins from X-ray solution scattering. *Biophys J.* 2001; 80:2946–2953. [PubMed: 11371467]
- Takekawa M, Tatebayashi K, Saito H. Conserved docking site is essential for activation of mammalian MAP kinase kinases by specific MAP kinase kinase kinases. *Mol Cell.* 2005; 18:295–306. [PubMed: 15866172]
- Tanoue T, Nishida E. Molecular recognitions in the MAP kinase cascades. *Cell Signal.* 2003; 15:455–462. [PubMed: 12639708]
- Tsutakawa SE, Hura GL, Frankel KA, Cooper PK, Tainer JA. Structural analysis of flexible proteins in solution by small angle X-ray scattering combined with crystallography. *J Struct Biol.* 2007; 158:214–223. [PubMed: 17182256]
- Wan PT, Garnett MJ, Roe SM, Lee S, Niculescu-Duvaz D, Good VM, Jones CM, Marshall CJ, Springer CJ, Barford D, Marais R. Mechanism of activation of the RAF-ERK signaling pathway by oncogenic mutations of B-RAF. *Cell.* 2004; 116:855–867. [PubMed: 15035987]
- Wang X, Tournier C. Regulation of cellular functions by the ERK5 signalling pathway. *Cell Signal.* 2006; 18:753–760. [PubMed: 16376520]
- Wang Z, Harkins PC, Ulevitch RJ, Han J, Cobb MH, Goldsmith EJ. The structure of mitogen-activated protein kinase p38 at-2.1 Å resolution. *Proc Natl Acad Sci U S A.* 1997; 94:2327–2332. [PubMed: 9122194]
- Wroblewski ST, Doweiko AM. Structural comparison of p38 inhibitor-protein complexes: a review of recent p38 inhibitors having unique binding interactions. *Curr Top Med Chem.* 2005; 5:1005–1016. [PubMed: 16178743]
- Xie X, Gu Y, Fox T, Coll JT, Fleming MA, Markland W, Caron PR, Wilson KP, Su MS. Crystal structure of JNK3: a kinase implicated in neuronal apoptosis. *Structure.* 1998; 6:983–991. [PubMed: 9739089]
- Yoon S, Seger R. The extracellular signal-regulated kinase: multiple substrates regulate diverse cellular functions. *Growth Factors.* 2006; 24:21–44. [PubMed: 16393692]
- Zarubin T, Han J. Activation and signaling of the p38 MAP kinase pathway. *Cell Res.* 2005; 15:11–18. [PubMed: 15686620]
- Zhang F, Strand A, Robbins D, Cobb MH, Goldsmith EJ. Atomic structure of the MAP kinase ERK2 at 2.3 Å resolution. *Nature.* 1994; 367:704–711. [PubMed: 8107865]
- Zhang X, Gureasko J, Shen K, Cole PA, Kuriyan J. An allosteric mechanism for activation of the kinase domain of epidermal growth factor receptor. *Cell.* 2006; 125:1137–1149. [PubMed: 16777603]

- Zhou T, Raman M, Gao Y, Earnest S, Chen Z, Machius M, Cobb MH, Goldsmith EJ. Crystal structure of the TAO2 kinase domain: activation and specificity of a Ste20p MAP3K. *Structure*. 2004; 12:1891–1900. [PubMed: 15458637]
- Zhou T, Sun L, Humphreys J, Goldsmith EJ. Docking interactions induce exposure of activation loop in the MAP kinase ERK2. *Structure*. 2006; 14:1011–1019. [PubMed: 16765894]

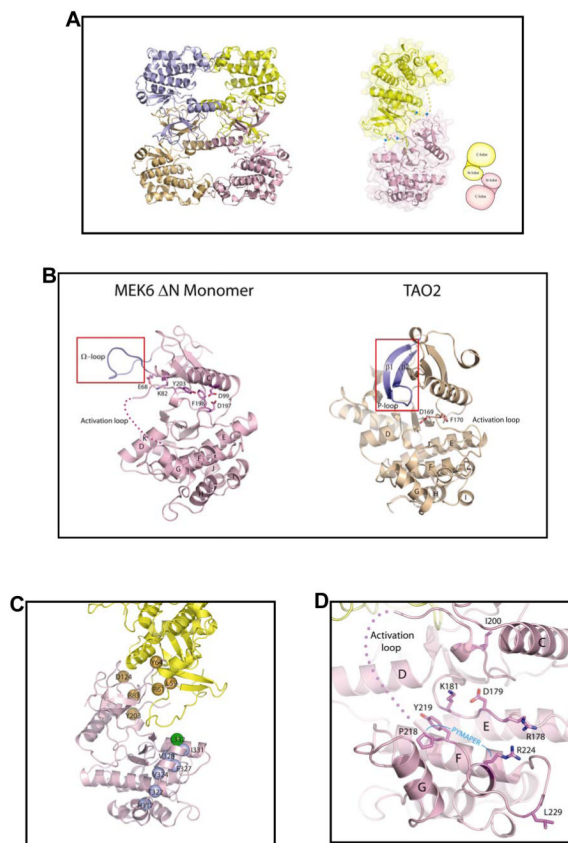


Figure 1. The structure of MEK6 /ΔN/DD

A: Left panel shows the two dimers in the asymmetric unit; and the center panel shows one of the crystallographic dimers. The two monomers are in yellow and pink. The disordered activation loop is shown in dotted line. **B:** A Monomer is depicted with the side-chains of residues Glu68, Lys82, Asp99, Asp197, Phe198 and Tyr203 represented in ball and stick. TAO2 structure in the same orientation is shown here for comparison. The red box highlights the Ω-loop in MEK6/ΔN/DD and compares it with β1-strand, and β2-strand enclosed in red box in TAO2. **C:** Close-up view of the C-terminus, helices J and K. Residues in the “DVD” motif are shown as yellow spheres, His317, Thr322, Val324, Phe327, Val328, and Ile331. We mutated the residues in the dimer interface, Asp124, Tyr64, Arg83, Arg61, Leu59 and Tyr203 (shown as orange spheres) to alanine. Leu332 (green sphere) is in the DVD motif and was also mutated. Note that the second subunit of the dimer is nearby (in yellow). **D:** Close-up view of the activation loop and PYMAPER loop in the same color scheme as in A. Arg178, Asp179, Lys181, Pro218, Tyr219, Leu229 and Arg224. Drawn in Pymol (DeLano, 2002).

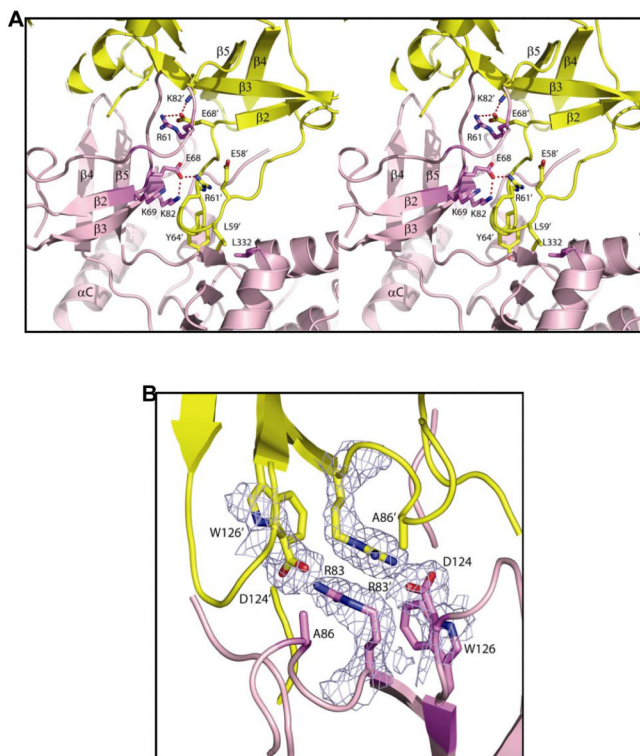


Figure 2. The dimer interface

A: Stereo view of the two Ω -loops bound to the opposite subunit active sites, and contacts with C-terminus. Two subunits shown, and rendered in cartoon. Side chains of Leu59, Arg61, Tyr64, Leu332, backbone of Gly60 and Arg61 rendered for both monomers. Dotted lines denote hydrogen bonds (2.8-3.0 Å) and **B.** View 180° rotation about Y from panel **A** showing the Arginine Stack. Arg83 and Ala86 Asp124 and Trp126 are rendered in ball and stick. Electron density contoured at 1σ covers selected side-chains.

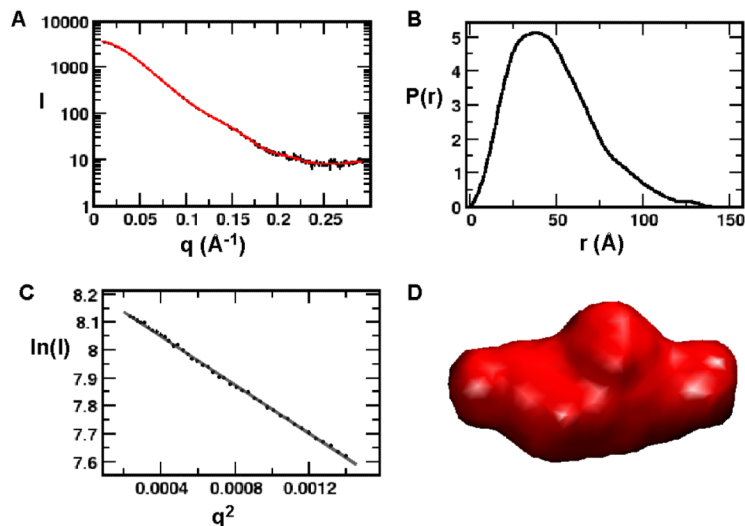


Figure 3. Low angle x-ray scattering of MEK6/ΔN/DD

A. Buffer-subtracted scattering profile (black) of the MEK6/ΔN/DD is consistent with an extended conformation. The fit to the experimental data of one *ab initio* DAMMIN model is shown in red. **B.** The electron pair distribution function of the experimental data shows a general bell-shaped curve, but with an asymmetric biased toward the longer distances, indicating an extended structure. D_{max} was 140 Å. **C.** Data in the Guinier region is linear, indicating monodispersity of the sample in solution. **D.** Averaged and filtered *ab initio* shape prediction for MEK6/ΔN/DD in solution was calculated by the program DAMMIN and aligned using the DAMAVER program suite. The overall volume is consistent with two molecules of MEK6/ΔN/DD and the crystallographically observed dimer.

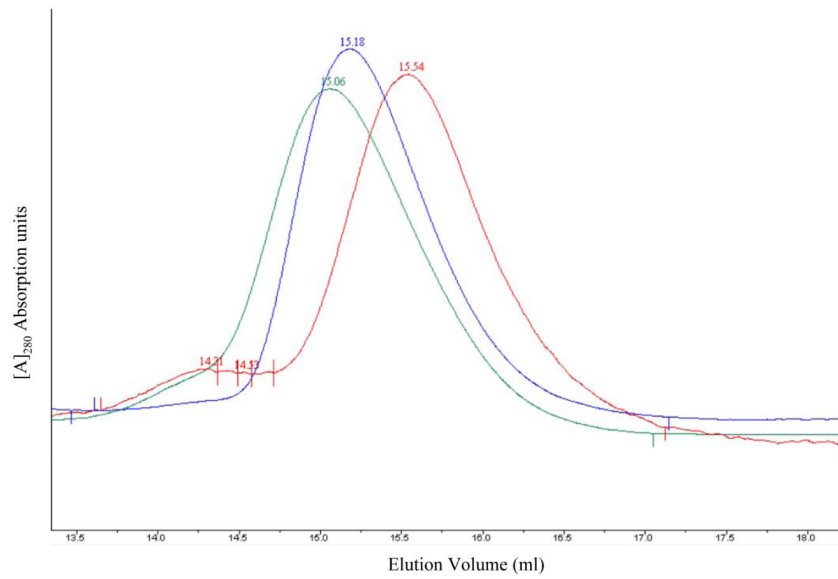


Figure 4. Comparison of elution volumes from analytical gel-filtration (Superdex 200 10/300) of MEK6/ Δ N/DD in the presence (red) and absence (green) of ATP in the column buffer and a double mutant D124A/W126S (blue). A shift toward lower molecular weight in the presence of ATP and for the double mutant indicates a change in dimer-monomer equilibrium.

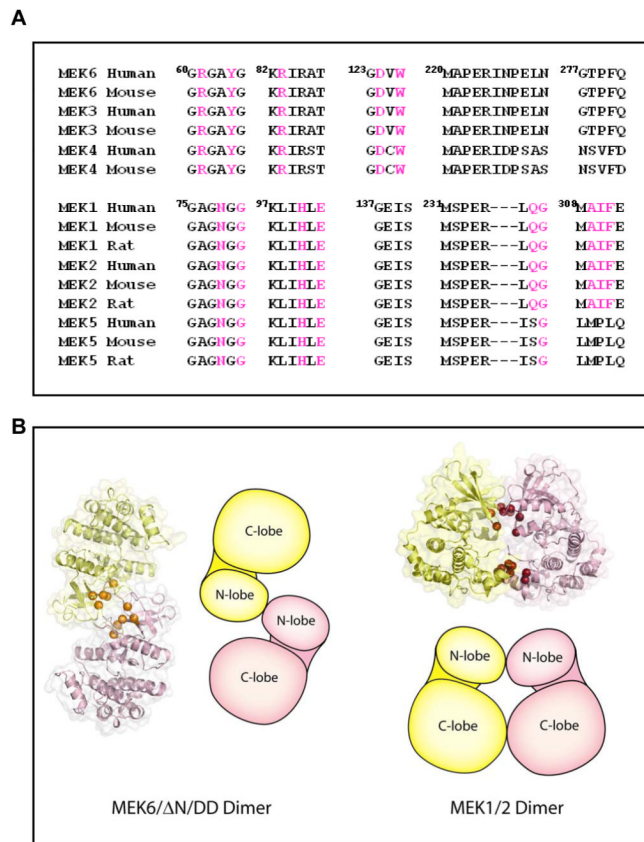


Figure 5.

A. Sequence alignments of MAP2Ks in regions forming the dimer interfaces in MEK6 and MEK1/2. **B.** The MEK6 dimer, with conserved interface residues rendered as balls. **C.** the MEK1/2 dimer from (Ohren et al) (PDB file 1S9J). A cartoon representation shows the differences in packing of the dimers in the two MAP2Ks.

Table 1

Statistics of crystallographic data and refinement

Space group	P3 ₂ 21
Unit cell dimensions (Å)	<i>a</i> = <i>b</i> =122.66, <i>c</i> =195.54
Wavelength (Å)	0.97905
Resolution (Å)	20-2.35
No. of unique reflections	71376
Average Multiplicity(last shell)	6.6(6.4)
Completeness (%) (last shell)	99.9(99.9)
Intensity <i>I</i> / σ <i>I</i> (%)	35/1.7
<i>R</i> _{sym} (last shell) ^a	0.07 (0.68)
<i>R</i> _{work} / <i>R</i> _{free} ^b	0.206/0.257
Non-H protein atoms	8835
Waters	331
RMSD in bond length (Å) ^c	0.02
RMSD in bond angles(°) ^c	2.00
Average B-values (Å ²)	57.2
Ramachandran plot statistics (%)	
Residues in most favored region	89.1
Residues in additionally allowed region	9.1
Residues in generously allowed region	1.8
Residues in disallowed region	0.0

$$^a R_{\text{sym}} = \frac{\sum |I_{\text{avg}} - I_j|}{\sum I_j}$$

^b $R_{\text{factor}} = \frac{\sum |F_o - F_c|}{\sum F_o}$, where F_o and F_c are observed and calculated structure factors, respectively, R_{free} was calculated from a randomly chosen 5% of reflections excluded from the refinement, and R_{work} was calculated from the remaining 95% of reflections.

^c RMSD is the root-mean-square deviation from ideal geometry.